Optical tweezers reveal relationship between microstructure and nanoparticle penetration of pulmonary mucus

Julian Kirch, Andreas Schneider, Bérengère Abou, Alexander Hopf, Ulrich F Schaefer, Marc Schneider, Christian Schall, Christian Wagner, Claus-Michael Lehr

Optical tweezers reveal relationship between microstructure and nanoparticle penetration of pulmonary mucus

Julian Kirch[a,1], Andreas Schneider[b,1], Bérengère Abou[c], Alexander Hopf[d], Ulrich F. Schaefer[a], Marc Schneider[a], Christian Schall[d], Christian Wagner[b,2], and Claus-Michael Lehr[a,e,2]

Departments of [a]Biopharmaceutics and Pharmaceutical Technology and [b]Experimental Physics, Saarland University, D-66123 Saarbruecken, Germany; [c]Labaratoire Matière et Systèmes Complexes, Paris-Diderot University, F-75205 Paris, France; [d]Fresenius Medical Care Deutschland GmbH, D-66606 St. Wendel, Germany; and [e]Department of Drug Delivery, Helmholtz Institute for Pharmaceutical Research Saarland (HIPS), Helmholtz Centre for Infection Research (HZI), D-66123 Saarbruecken, Germany

Edited by David A. Weitz, Harvard University, Cambridge, MA, and approved September 19, 2012 (received for review August 27, 2012)

In this study, the mobility of nanoparticles in mucus and similar hydrogels as model systems was assessed to elucidate the link between microscopic diffusion behavior and macroscopic penetration of such gels. Differences in particle adhesion to mucus components were strongly dependent on particle coating. Particles coated with 2 kDa PEG exhibited a decreased adhesion to mucus components, whereas chitosan strongly increased the adhesion. Despite such mucoinert properties of PEG, magnetic nanoparticles of both coatings did not penetrate through native respiratory mucus, resisting high magnetic forces (even for several hours). However, model hydrogels were, indeed, penetrated by both particles in dependency of particle coating, obeying the theory of particle mobility in an external force field. Comparison of penetration data with cryogenic scanning EM images of mucus and the applied model systems suggested particularly high rigidity of the mucin scaffold and a broad pore size distribution in mucus as reasons for the observed particle immobilization. Active probing of the rigidity of mucus and model gels with optical tweezers was used in this context to confirm such properties of mucus on the microscale, thus presenting the missing link between micro- and macroscopical observations. Because of high heterogeneity in the size of the voids and pores in mucus, on small scales, particle mobility will depend on adhesive or inert properties. However, particle translocation over distances larger than a few micrometers is restricted by highly rigid structures within the mucus mesh.

forced penetration | pulmonary drug delivery | cryoelectronmicroscopy

Mucus is a complex fluid of spatially varying properties containing hydrogel-forming glycoproteins (mucins) that enable the exchange of nutrients, provide lubrication, and protect the body from environmental influences. A compact layer of this hydrogel covers the complete gastrointestinal tract, the urogenital tract, and the epithelium of the upper and central airways of the lung. Here, the highly viscous, several micrometers-thick layer of mucus rests on a layer of lower viscosity and watery consistency, the pericilliary layer. This layer enables efficient cilliary beating by allowing only the tips of the cilia to penetrate into the mucus. Notably, the beating cilia do not affect the structure of mucus in any significant way (1, 2). The barrier function of mucus is of special importance, particularly to pharmaceutical research. Translocation of particulate matter, such as dust, pathogens like viruses, or pharmaceutical (nano) carriers, through this barrier is currently under investigation but still not completely understood. This lack of understanding also holds true for the active mucus penetration of immunocompetent cells, such as airway macrophages, which will, therefore, not be considered herein (3, 4). In contrast to pathogens or toxic agents, penetration of this mucus barrier is strongly desired for any kind of drug delivery device, such as (nano)particulate application systems. Here, modification of particles with PEG was reported to enhance particle diffusivity within the probed timeframe. On the contrary, chitosan is established as mucoadhesive and often applied to increase mucosal bioavailability; thus, it may decrease particle diffusivity.

Recently, the investigation of the microrheology of mucus in this context has been gaining momentum (5). In particular, the discrimination between different filtering effects, their correlation with gel structure, and additional details on how such filtering is controlled are being investigated (6). Furthermore, the influence of electrolytes, such as bile salts, on particle mobility in mucus is tackled (7). The most established parameters to describe filtering effects are pore size (8) and particle–mucus interactions (9). The pore size is derived from either imaging data or particle tracking experiments. Particle tracking also provides information on mucociliary clearance (1) and particle interactions with components of the mucus' polymer mesh (e.g., adhesion to mucins). Current studies in this field either focus on pore size as limiting factor (10, 11) or suggest the more complex interaction filtering of mucus rather than size exclusion effects (6). Concerning noncryogenic microscopic imaging, a disadvantage of such methods is their susceptibility to artifacts because of their harsh conditions, staining, or sputtering. Particle tracking experiments, however, suffer from limitations in short correlation time, small observed area, or both. Alternatives to such small-scale mobility of particles in mucus are classical diffusion chamber studies, which quantify translocated particle fractions (8). Those studies, however, do not provide information about microscopic particle behavior and mucus structure.

Therefore, despite being extensively investigated, the major problem in this field is the missing link between penetration behavior on scales larger than a few micrometers, microrheology, and structure of this complex fluid. The present study bridges this gap through the combination of advanced methods, which to our knowledge, has not been applied in this context. Initially, we investigate particle–mucus interactions by atomic force microscopy to quantify adhesion of differently coated nanoparticles to mucus components to confirm mucus interaction properties of the applied particles. Penetration of particles through mucus and model gels is investigated by quantifying penetration velocity of magnetic particles through these capillaries. Penetration behavior is assessed considering the theory of particle mobility in a distinct force field.

Author contributions: J.K., A.S., U.F.S., M.S., C.S., C.W., and C.-M.L. designed research; J.K., A.S., and A.H. performed research; B.A. contributed new reagents/analytic tools; J.K. and A.S. analyzed data; and J.K., A.S., U.F.S., M.S., C.W., and C.-M.L. wrote the paper.

The authors declare no conflict of interest.

This article is a PNAS Direct Submission.

[1]J.K. and A.S. contributed equally to this work.

[2]To whom correspondence may be addressed. E-mail: c.wagner@mx.uni-saarland.de and lehr@mx.uni-saarland.de.

This article contains supporting information online at www.pnas.org/lookup/suppl/doi:10.1073/pnas.1214066109/-/DCSupplemental.

This macroscopic particle mobility is correlated to microscopic mucus rheology and structure. Here, we apply cryogenic scanning EM (cryo-SEM), which allows for an unbiased determination of the native mucus structure. Furthermore, optical tweezers are used to passively and actively probe native respiratory mucus. This approach is unique in this context and shows that a crucial point in particle mobility is not only the pore size distribution but also mucin scaffold rigidity, which is not captured in regular methods of measuring mucus rheology. The combination of pore size and rigidity can be used to explain the mentioned discrepancies between micro- and macrorheology of mucus as well as between low long-distance mucus penetration and previously observed microscopic particle mobility.

Results and Discussion

Atomic Force Microscopy (AFM). Determination of adhesive interactions between mucin fibers and nanoparticles of different surface chemistry (Fig. S1) could be realized by force spectroscopy. Measurements of adhesion forces between nanoparticles and silica substrate allowed for an unbiased comparison between chitosan and PEG-coated (2 kDa) polystyrene (PS) nanoparticles. Particle adhesion to mucin fibers attached to the tip of the cantilever compared with their adhesion to the substrate shows that chitosan-coated particles adhere much stronger to the fibers than PEG-coated particles. Whereas the adhesion force between a mucin-functionalized tip and chitosan-coated particles was over 250% stronger than the adhesion force to the substrate, PEG coating of nanoparticles resulted in an even reduced adhesion compared with the bare silica substrate (Fig. S2). This finding is in agreement with previous studies that observed similar effects. Adhesive interactions between mucin fibers and differently coated nanoparticles were investigated through quantification of mucin adsorption to these particles. In such studies (12), PEGylation was shown to reduce mucin adsorption and thus, adhesion. Surface chemistry was also shown to strongly influence short-term particle diffusion in cervical or gastrointestinal mucus in several previous studies (13, 14). In contrast, chitosan coating is typically applied to increase the interactions (15). We applied a method developed a few years ago (16) to probe long-distance/long-term particle mobility to increase the proximity to the in vivo situation. Here, particle mobility in mucus is investigated for time scales and spatial distances of higher physiological relevance.

Capillary Penetration Experiments. Penetration of magnetic particles over macroscopic distances in mucus and model gels was investigated using the method in the work by Kuhn et al. (16). This method allowed for the analysis of direct translocation and penetration behavior of differently coated magnetic nanoparticles over defined distances in mucus and model systems. Investigation of penetration behavior over such distances may predict the potential of particles to translocate through thick physiological mucus barriers better than other methods.

To show the feasibility of the method and perform a proof-of-concept experiment, capillary experiments were conducted with hydroxyethylcellulose (HEC) gels as a model system with a relevant molecular weight (17). In principle, HEC was chosen because of its chemical similarity to mucins and its microrheologically similar behavior (additional details in *SI Text*). Therefore, HEC gels were suitable as a model system. Here, gradual transition from water to dense hydrogels was realized by applying HEC gels of gradually increasing concentration and thus, gradually increasing viscosity and elasticity. Penetration experiments were conducted with both types of particles that penetrated HEC, allowing for a calculation of penetration velocities (Fig. 1, *Upper Right*). As expected, it was shown that penetration velocity was, indeed, strongly dependent on rheological properties and polymer concentration of the model gel (Fig. 1, *Lower Right*). Penetration velocities of the particles in the HEC gel of the highest concentration

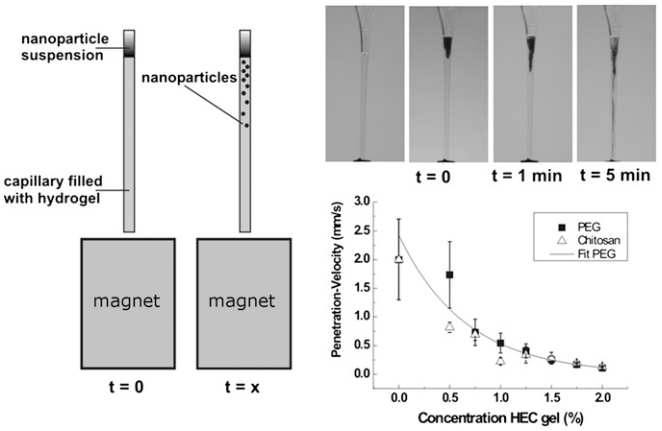

Fig. 1. Scheme of capillary penetration experiments (*Left*). Penetration of PEGylated and chitosan-coated magnetic nanoparticles through 1% HEC gel within 5 min (*Upper Right*). Penetration velocity is inversely related to gel viscosity and thus, polymer concentration, which can be fitted with the model in the work by Chrambach and Rodbard (19) ($R^2_{PEG} = 0.93$). Adhesion of chitosan-coated particles to cellulose fibers can be confirmed by the drop in penetration velocity (*Lower Right*). Data are mean ± SD.

decreased to approximately one-tenth of the initial value as measured in water. Correlation of particle velocity with polymer concentration of the respective hydrogel can be used to assess the accordance of penetration behavior with theoretical models describing particle mobility in a force field (e.g., electrostatic or magnetic). Fitting of penetration velocities with the model (18) in the work by Chrambach and Rodbard (19) (additional details in *SI Text*) shows that, in general, sufficient congruence can be reached for the penetration behavior of PEG particles ($R^2_{PEG} = 0.93$), which exhibits greater conformity with the mentioned model than penetration behavior of chitosan-coated nanoparticles. Here, a fit with sufficient goodness could not be achieved. This result may be because of the fact that chitosan-coated particles, similar to mucins, interact adhesively with HEC fibers. The fact that the applied model incorporates inert (i.e., nonadhesive) particles as a boundary condition may, therefore, be the reason for the greater goodness of the fit for PEGylated particles. This finding is consistent with the nonadhesive properties of PEGylated particles as displayed in Fig. S2. These results show that discrimination between the applied particle types regarding their penetration velocity is, indeed, possible by this method. Because HEC fibers are polysaccharides, chemical similarities to polysaccharide side chains of mucins over large areas cannot be doubted. Thus, HEC gels mimic mucus gel and its adhesion to chitosan or chitosan-coated particles. This adhesive interaction is supposed to be largely caused by electrostatic interactions (20). Furthermore, the model (18) in the work by Chrambach and Rodbard (19) allows for an estimation of the average pore size of the gel. According to this model, the pore size equals the size of the probe particles when penetration velocity drops to 50% of its initial value. Considering the fit of penetration velocity of PEGylated particles, this finding means that the average pore size of HEC gels should be ~200 nm for concentrations around 0.5%.

Performing the same experiments with native respiratory mucus, we were surprised to find that mucus is, indeed, a tenacious fluid (21). No penetration through could be observed, not even into the mucus column (Fig. 2). This finding was true even for very long exposure (>3 h) to the magnetic field. A difference between chitosan-coated and PEGylated nanoparticles in this behavior could not be observed at any time. Any remaining small differences in penetration behavior that cannot be resolved in this setup will not play a significant role in the physiological situation, because residence time of deposited nanoparticles on the moving

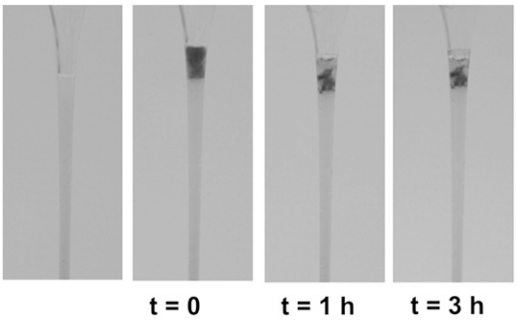

Fig. 2. Magnetic PEG-coated nanoparticles do not penetrate into a mucus-filled column, even within incubation times longer than 3 h.

mucus blanket is rather short (1). This indifference to the particle type might be enhanced by the native mucus containing proteins, lipids, and surfactants. The interaction with these components, especially phospholipids and proteins, may reduce the differences between the particles' surface chemistry, which was recently reported for the deep lung (22). The fact that both types of particles did show a distinctive penetration through HEC gels but no penetration through mucus required a detailed investigation of the two hydrogels. Therefore, the structure of native respiratory mucus and HEC gels was analyzed by cryo-SEM imaging.

Imaging with Cryo-SEM. Structural analysis of mucus and HEC gels was performed with cryo-SEM. The structure of the polymer matrix of mucus and the differently concentrated HEC gels could be imaged in their native state with high resolution (Fig. 3). Pore size could be determined to range between ~100 and 500 nm in HEC of 0.5% concentration (Fig. 3 *A* and *B*). With increasing polymer concentration, HEC hydrogels exhibit decreasing pore sizes as the polymer mesh becomes more condensed (Fig. 3*C*). The average thickness of the polymer scaffold can be determined to be ~20 nm. These measurements could confirm the findings presented in *Capillary Penetration Experiments*. Indeed, a pore size approaching the diameter of the penetrating particles (~200 nm) can be expected to be HEC gel concentrations between 0.5% and 1%, which were predicted by the model in the work by Chrambach and Rodbard (19). Cryo-SEM imaging of mucus gel revealed a very different structure of the polymer mesh: large pores are heterogeneously combined with very small pores. Pore sizes of mucus ranged between ~100 nm and voids of several micrometers in diameter (Fig. 3*D*). Furthermore, thickness of polymer scaffold could be determined to be much higher than in HEC gels (Fig. 3*E*).

Cryo-SEM images illustrate two considerable features of the mucus hydrogel that may have an impact on particle mobility and penetration in this polymer mesh: the pore size distribution and the thickness of the polymer scaffold. Gel structure, including pore size distribution with large but also very small voids, is heterogeneous in mucus, which is in accordance with recent findings for cervical mucus (23). Comparison of cryo-SEM images of HEC gels with the results from capillary penetration experiments, however, shows that pore size is not always the limiting factor for penetration (for HEC gels, particles penetrate a polymer mesh with pores much smaller than the particle diameter). Therefore, considering that particles did not penetrate mucus as presented in *Capillary Penetration Experiments*, one would postulate either a high rigidity of the mucin scaffold that resists any rupture or deformation on application of external forces (e.g., a magnetic field); therefore, particles are, indeed, captured in the smaller pores or confined by strong adhesive interactions between particles and mucus (interaction filtering). Whether rupture or deformation occurs cannot be distinguished. The observation of the thick polymer scaffold as described above and the fact that mucoinert PEGylated particles did not show better penetration into mucus suggest that the former may be the dominant mechanism here. The very thick polymer scaffold in mucus (Fig. 3*E*) may be composed of thick mucin bundles, which was suggested by an earlier study (23). Regarding the effect of fluid dynamics of the transported mucus blanket on such a structure, it can be hypothesized that overall morphology and structural parameters of the mucus mesh will not be affected. This result is because of the fact that, within the mucus blanket, there exists only a negligible relative flow, which was shown in

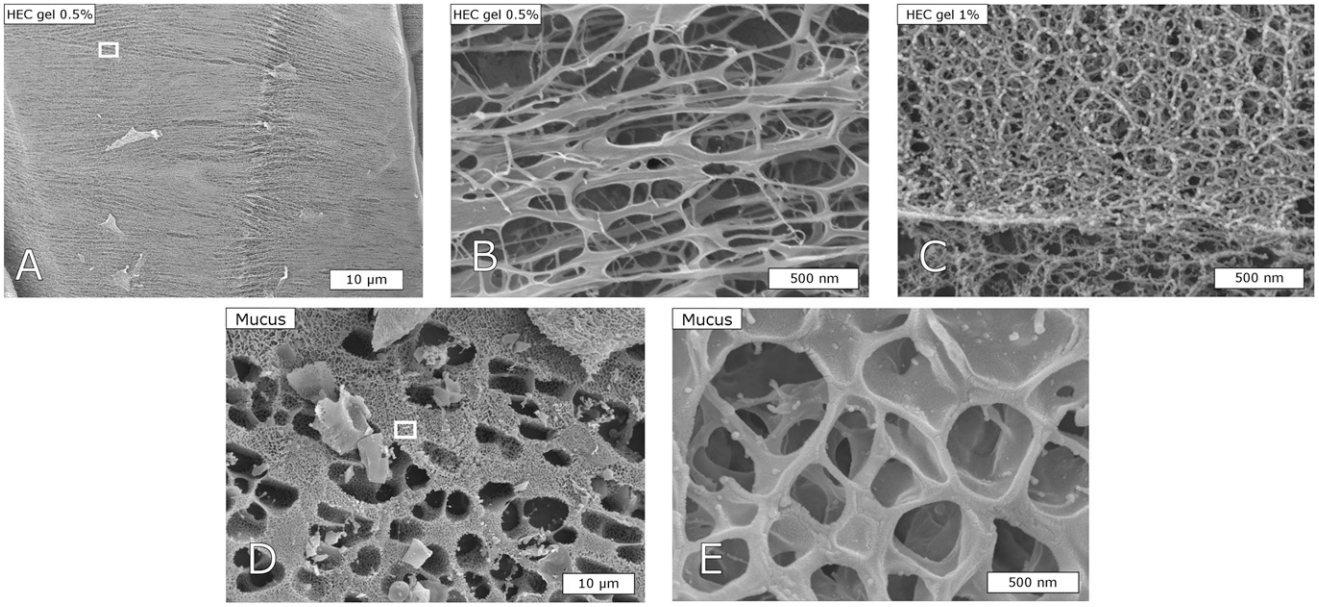

Fig. 3. Representative cryo-SEM images of HEC hydrogels (*A*–*C*) and mucus (*D* and *E*). Increase in polymer concentration from 0.5% (*A* and *B*) to 1% (*C*) leads to a strong decrease in hydrogel pore size. Cryo-SEM images of mucus showed the strongly heterogeneous nature of mucus polymer mesh. Large as well as very small pores can be observed (*D*). Furthermore, the polymer scaffold of mucus is excessively thicker than the polymer scaffold in HEC gels. (Scale bar: *A* and *D*, 10 μm; *B*, *C*, and *E*, 500 nm.) Additional micrographs can be found in Fig. S3.

previous experiments and computational studies (1, 2, 24). The consequences of such rigid and thick polymer structures are also assessed by optical tweezers below.

In summary, to describe mobility of particles in mucus, both size sieving effects and interaction filtering have to be considered; however, they have been considered only in addition to the evaluation of the mechanical properties of the polymer scaffold. The results described above show that the key feature of mucus could be its highly rigid structure in conjunction with the observed heterogeneous pore size distribution of very small but also, large pores. Assessment of the first point was performed with optical tweezers, which is an advanced tool to study active microrheology in a noninvasive way.

Passive Microrheology and Active Probing of the Microstructure by Optical Tweezers. Optical tweezers were applied to probe the microrheology and particularly, the rigidity of the polymer scaffold in a noninvasive way on the micrometer scale. Native respiratory mucus as well as the HEC model gel were analyzed with stationary and oscillating optical traps. In the case of the stationary passive tracking experiment, a single bead was confined to a small spatial volume, and the displacement from the center of the trap was recorded. Afterward, the mean squared displacement (MSD) was calculated (Fig. 4). In contrast to purely viscous, Newtonian fluids, where the MSD is proportional to time, for complex fluids like polymers, additionally elastic behavior becomes apparent; the history of former deformations plays an important role in its flow properties, which leads to deviations from the linear behavior of the MSD in favor of power law or an even more complex functional behavior. By plotting the 1D MSD of the beads out of the center of the optical trap against the correlation time, the properties of mucus and the HEC model gel are determined (Fig. 4). The data cutoff for long times was chosen at the point where the MSD reached a plateau-like maximum defined by the constrictions caused by the optical trap. Extensive heterogeneity of mucus morphology, as suggested by cryo-SEM studies, could be confirmed. Highly diverse slopes of the MSD of particles in mucus dependent on correlation time indicate strongly varying local properties (Fig. 4*A*). Furthermore, the spread in absolute values suggests a large variety in particle mobilities that spans more than an order of magnitude at all observable correlation times. In addition, these heterogeneities can even be observed on the same spot in different directions along the x and y axes (more information in *SI Text* and Fig. S4), indicating anisotropic rheological properties. Contrary to mucus, the curve progression of the MSD that was observed in HEC shows only minor deviations between different positions within its scaffold, thus showing high spatial homogeneity. Additional evaluation of the MSD and the corresponding shear moduli is given in *SI Text*. However, neither the MSD nor the shear modulus of mucus and HEC gives any information about the deviating macroscopic penetration behavior of particles in both materials. According to the fluctuation data, both materials should react similarly, at least on a microscopic scale. To grasp these seemingly contradictory properties, experiments investigating the viscoelastic behavior of actively displaced particles had to be performed.

A bead was caught in the trap, and the piezoelectric stage on which the probe cell rested was moved in a triangular wave pattern. The motion of the stage and the displacements of the bead relative to the center of the trap were recorded. It could be shown that trapped particles can easily be moved through HEC gels as the particle follows the moving trap (Fig. 5*B*) (i.e., the force exerted on it by the laser is sufficient to distort, stretch, or possibly rupture the polymer scaffold of dense HEC gels). On the contrary, active measurements within mucus (Fig. 5*A*) showed that most beads could not be moved significantly, showing the high rigidity of the polymer scaffold. Again, heterogeneity in morphology of mucus structure was confirmed, because a few particles could be displaced easier (more information in *SI Text* and Fig. S5). Those particles may be located in one of the earlier-mentioned larger voids inside mucus, and on a deflection of the optical trap of more than 2 μm, they either do not make contact with the walls or are only partially in contact with them. In the second case, it seems like a tether of mucus is fixed to the bead and displaced together with it, which leads to an easy displacement up to certain distances, but as soon as these distances are exceeded, the bead is pulled back to its equilibrium position near the wall. Within these larger pores (Fig. 3*D*), the bead senses a medium of low viscosity; at some locations, this medium is even similar to water. This diversity in the behavior of beads during active displacement dependent on the position of the particle within mucus is coherent with the highly diverse MSD slopes observed by the passive tracking experiments and the extensive heterogeneity in morphology. Particles may be tightly immobilized in smaller pores or more mobile in larger pores. Therefore, a certain distribution of pore sizes in mucus may be the reason for a broad statistical spread of its rheological behavior (Fig. 4*A*). Although particles in HEC can be moved much easier by external forces, no comparably large pores exist within the material. This finding results in a much more homogeneous material response, although the elastic as well as the viscous modulus measured by passive tracking experiments in the setup of optical tweezers show comparable or even bigger values depending on the excitation frequency (Fig. S6). Thus, although the MSD may, in some cases, pretend a high particle mobility, macroscopic penetration experiments and active particle deflection by optical traps challenge this result. In other cases (e.g., HEC gels), particles can be driven actively through the fluid despite the MSD, indicating an at least equal confinement. As sketched in Fig. 6, particles in HEC

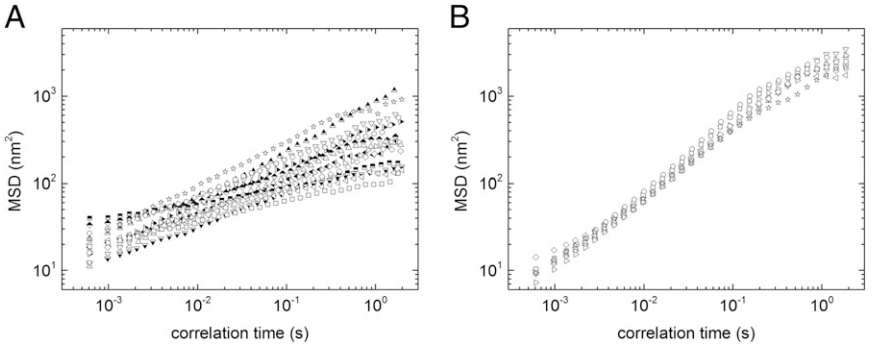

Fig. 4. MSDs from passive tracking experiments at varying positions (denoted by different symbols) within (*A*) mucus and (*B*) HEC. Contrary to HEC gels, mucus shows highly diverse curve progressions, indicating a heterogeneous structure and pore size distribution of the polymer scaffold. The strength of the optical trap was chosen for all measurements between 3 and 8 pN/μm.

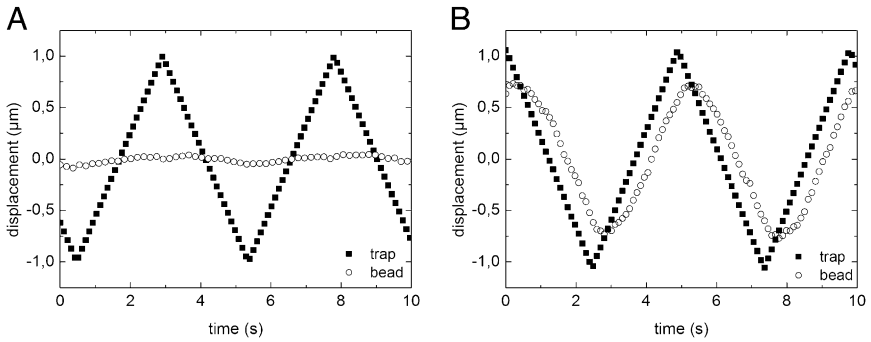

Fig. 5. Displacement of the optical trap (■) and the position of the trapped bead (○) with respect to time during an active measurement. although the bead is unable to react significantly to the oscillating motion of the trap within mucus (*A*); in the HEC gel, the bead follows the trap with a slight phase shift and a dampened amplitude (*B*).

gels are dispersed in dense gels of small pore sizes. On actively displacing a bead, the polymer scaffold is deformed or even ruptured. In mucus, the mobility of particles depends on the local pore size. However, because of the polymer scaffold rigidity, they cannot be moved over large distances. Therefore, the investigation of the microrheology by passive particle tracking must not remain the sole method to extrapolate to particle translocations over larger distances (>5 μm), which is particularly true for tracking experiments with very short correlation times. It was shown in this study that a setup of optical tweezers is a reliable tool to determine not only the microrheology of a material but also the auxiliary parameters, such as pore rigidity and size on the micrometer scale.

Conclusion

A combination of tools, such as cryo-SEM, capillary penetration, and optical tweezers, was applied to assess particle mobility in and penetration through mucus and model hydrogels on various length scales. It could be shown that the thorough assessment of particle penetration through mucus cannot be described solely by methods focusing on only one scale, be it micro-, meso-, or macroscopic behavior, like most current studies focusing on particle mobility in biological fluids. It was shown that neither the particle–mucus interactions nor the pore size of the hydrogel alone is sufficient to describe particle mobility in mucus. HEC hydrogels with much smaller pore sizes and a higher elastic and viscous modulus were even shown to be penetrated more easily by magnetic particles than mucus. It was discovered that this discrepancy may be caused by differences in rigidity of the polymer scaffold, which was assessed by optical tweezers, and a broad pore size distribution in mucus. The previously observed differences in particle mobility of differently coated beads may, thus, be caused by differences in particle adhesion in larger voids of mucus. Therefore, this study presents the so far missing link between microrheology and macroscopical observations regarding particle mobility in mucus.

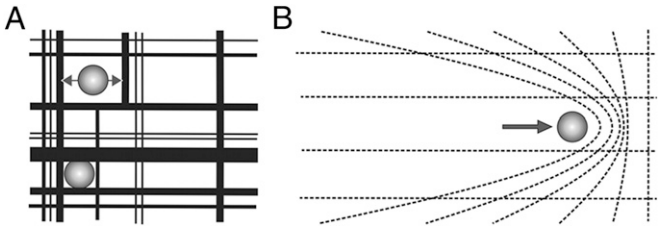

Fig. 6. Particles in HEC gels may be moved by external forces (*B*); because of the rigidity of the polymer scaffold, the confinement of particles in mucus is stronger (*A*) and prevents large displacements. However, if placed in larger voids, particles show some measure of mobility on small length scales.

Materials and Methods

Materials. All particles were obtained from commercial sources. In atomic force microscopy, we used polystyrene particles with covalently linked coating (chitosan and 2 kDa PEG, 500 nm diameter; Kisker Biotech). Capillary penetration experiments were conducted with dextran iron oxide composite particles with covalently linked coating (chitosan and 2 kDa PEG) with a diameter of 170–200 nm (Micromod). For the experiments with the optical tweezers, either polymethacrylate beads with a size of 4 μm or melamine resin beads (Fluka) with a size of 5 μm were used. Detailed information on particle characterization is in *SI Text*. For the observation of the samples in the setup of optical tweezers, a Gene Frame (ABgene; Epsom), a special sample cell with a low volume of 25 μL, was necessary. All chemicals used were of analytical grade. Water used was always Milipore water.

Atomic Force Spectroscopy. AFM cantilevers were cleaned and modified according to a previously described procedure (25). In short, cantilevers were cleaned two times in piranha etch (97% H_2SO_4 in 30% H_2O_2; 1:1), rinsed in water, and dried under nitrogen flow. Cantilevers were suspended in silane solution (1% 3-glycidyloxypropyl-trimethoxysilane and 0.5% *N*-ethyldiisopropylamine in water-free toluene) for 4 h at room temperature to form a self-assembled monolayer, providing a hydroxyl-reactive surface to primary hydroxyl groups of mucins. After silanization, cantilevers were rinsed two times for 20 min with dry toluene and dried under nitrogen flow. Subsequently, cantilevers were suspended overnight in 1% mucin solution followed by rinsing with water.

The sample substrate was silica, and it was cleaned like the cantilevers. A drop of particle suspension (chitosan or PEG-2000–coated polystyrene particles in water) was placed onto the substrate and dried in air. These samples were used in subsequent force imaging using a fluid cell.

Measurements of force plots were done by force volume imaging in an AFM (Multimode V; Bruker) in fluid conditions where a surface is scanned while recording force–distance plots for each pixel of the image. Force volume images (4,096 force plots per image) were taken of the samples with 10 nN trigger force and a surface dwell time of 1 s. Force plots attributed to the particles were extracted, analyzed, and compared with the force plots attributed to the substrate with Nanoscope 7.13 software (Bruker). The adhesion force was averaged over all force plots attributed to one particle. Several particles ($n \geq 6$) were analyzed, and the statistical variation in average adhesion force among the particles was considered as statistical error.

Capillary Penetration Experiments. Capillary penetration experiments were conducted according to a method recently introduced in the work by Kuhn et al. (16). Briefly, capillaries were filled with a model gel or respiratory mucus and sealed with vacuum grease on one end; 10 μL particle suspensions (chitosan/PEG-2000–coated magnetic dextran iron oxide composite particles) were pipetted on top of the gel column. Filled capillaries were placed upright with their sealed end in a reproducible position 2–4 mm from the pole of a neodymium magnet (detailed information on the magnetic field in *SI Text*). Velocity of the magnetic particles while being pulled through gel or mucus was obtained by measuring the traveling time of the particle. Native respiratory mucus was obtained from the distal region of the bronchia during bronchoscopy of four healthy horses and stored at −80 °C until use, because adequate human mucus is not available. According to previous studies, such storage conditions should not influence mucus rheological properties (26). Three separate samples of mucus from the same individual

were analyzed by this method. Model gel was pharmaceutical-grade hydroxyethylcellulose (HEC 370, molecular mass = 140 kDa; SE Tylose GmbH & Co. KG) of various concentrations. This specific molecular mass was chosen because of the fact that it mimics macroscopical rheological properties of mucus. To prepare the model gel, the respective amount of HEC was dissolved under overnight stirring in water.

Cryo-SEM. HEC hydrogels and native respiratory mucus were imaged by cryo-SEM. HEC gels were prepared by dissolving the respective amount of HEC in water. Before SEM imaging, HEC gels and mucus were collected in a thin dialysis capillary. Gel-filled capillaries were immediately frozen in liquid propane to only allow formation of amorphous water and circumvent formation of crystalline water. Capillaries were cut in smaller pieces to subsequently image the brim of the cut. Sublimation of frozen, amorphous water inside the porous HEC gel and mucus was carried out for 1 h at −100 °C (Baltec SCD 500 Sputter coater; Baltec/Leica). Subsequently, the surface of the dry polymer scaffold was sputter-coated with platinum (layer thickness ∼ 12 nm). After sputtering, samples were transferred into the SEM (DSM 982 Gemini; Zeiss) and imaged at −120 °C (5 keV, 5–6 mm working distance). To judge the interindividual differences, mucus from four horses was analyzed (Fig. S3). The inhomogeneous structure could be confirmed in each sample. Therefore, only images of one of these samples are depicted here (Fig. 3 *D* and *E*).

Optical Tweezers. HEC gels were prepared by dissolving the respective amount of HEC in water. In HEC ($n_m \sim 1.33$), polymethacrylate beads ($n_b = 1.49$) were used, whereas in mucus, melamin resin beads ($n_b = 1.68$) proved to be a good choice. For the preparation of the samples, ∼2–4 μL suspension (solid content of 10%) were mixed with about 100 μL fluid. The concentration of beads was chosen in a range of 200–2,000 ppm to avoid hydrodynamic interactions between multiple beads. All samples were vortexed for about 5 min to make sure that the beads were distributed homogeneously; 25 μL this mixture were filled into a container and sealed airtight with cover glasses and vacuum grease. Mucus samples of the same individual as presented in *Imaging with Cryo-SEM* (Fig. 3 *D* and *E*) were taken from the same batch on successive days. All samples were imaged within 4 h after the preparation process.

The setup of optical tweezers was identical with the setup used in the work by Ziehl et al. (27). The beam of a solid-state laser (Ciel; Laser Quantum) was guided to the oil immersion objective (N.A. = 1.4, 60× magnification) to create a harmonic trapping potential within the focal region of a microscope (Eclipse TE2000-S; Nikon GmbH). The visualization of trapped beads was achieved by illuminating the sample with a light emitting diode (LED) illumination source (ZLED CLS 9000; Zett Optics) from above in the inverse direction of the laser beam through the sample cell onto the chip of a high-speed camera (HiSpec 2G; Fastec Imaging). The beads were recorded for a duration of 16 s with a sample rate of 16,384 Hz and tracked afterward by the means of a cross-correlation algorithm realized in LabView 2011 (National Instruments Germany GmbH), which allowed for the determination of the particle displacements with a spatial resolution of ∼2 nm (28).

Two types of measurements were conducted. During a passive tracking experiment, a bead was held in place by the trap, and the Brownian motion was recorded as reported above. However, active experiments were performed by moving the piezoelectric stage of the setup in a triangular oscillation pattern induced by the signal of a waveform generator. The amplitude and frequency of the oscillation were chosen according to the mobility of the bead at its current position (usually between 1 and 4 μm and 0.1 and 0.2 Hz, respectively). The observation time was chosen in a way that at least two full oscillation periods could be recorded. Synchronous to image acquisition, the voltage signal driving the stage was recorded by a data acquisition card (National Instruments Germany GmbH). All measurements by optical tweezers were performed at 20 °C. During each measurement session, at least eight separate positions were investigated. At each position, two passive as well as two active experiments were performed. The oscillations during active experiments were directed perpendicularly to each other.

ACKNOWLEDGMENTS. We thank the German Research Association (DFG) within Priority Program LE 1053/16-1 and the German Graduate School GRK 1276 for financial support.

1. Kirch J, et al. (2012) Mucociliary clearance of micro- and nanoparticles is independent of size, shape and charge—an ex vivo and in silico approach. *J Control Release* 159(1): 128–134.
2. Smith DJ, Gaffney EA, Blake JR (2007) A model of tracer transport in airway surface liquid. *Bull Math Biol* 69(3):817–836.
3. Rothen-Rutishauser B, et al. (2010) Relating the physicochemical characteristics and dispersion of multiwalled carbon nanotubes in different suspension media to their oxidative reactivity in vitro and inflammation in vivo. *Nanotoxicology* 4(3):331–342.
4. Rothen-Rutishauser BM, Kiama SG, Gehr P (2005) A three-dimensional cellular model of the human respiratory tract to study the interaction with particles. *Am J Respir Cell Mol Biol* 32(4):281–289.
5. Lai SK, Wang YY, Wirtz D, Hanes J (2009) Micro- and macrorheology of mucus. *Adv Drug Deliv Rev* 61(2):86–100.
6. Lieleg O, Ribbeck K (2011) Biological hydrogels as selective diffusion barriers. *Trends Cell Biol* 21(9):543–551.
7. Macierzanka A, et al. (2011) Adsorption of bile salts to particles allows penetration of intestinal mucus. *Soft Matter* 7:8077–8084.
8. Sanders NN, et al. (2000) Cystic fibrosis sputum: A barrier to the transport of nanospheres. *Am J Respir Crit Care Med* 162(5):1905–1911.
9. Mura S, et al. (2011) Biodegradable nanoparticles meet the bronchial airway barrier: How surface properties affect their interaction with mucus and epithelial cells. *Biomacromolecules* 12(11):4136–4143.
10. Olmsted SS, et al. (2001) Diffusion of macromolecules and virus-like particles in human cervical mucus. *Biophys J* 81(4):1930–1937.
11. Dawson M, Wirtz D, Hanes J (2003) Enhanced viscoelasticity of human cystic fibrotic sputum correlates with increasing microheterogeneity in particle transport. *J Biol Chem* 278(50):50393–50401.
12. Yoncheva K, Lizarraga E, Irache JM (2005) Pegylated nanoparticles based on poly (methyl vinyl ether-co-maleic anhydride): Preparation and evaluation of their bioadhesive properties. *Eur J Pharm Sci* 24(5):411–419.
13. Lai SK, et al. (2007) Rapid transport of large polymeric nanoparticles in fresh undiluted human mucus. *Proc Natl Acad Sci USA* 104(5):1482–1487.
14. Crater JS, Carrier RL (2010) Barrier properties of gastrointestinal mucus to nanoparticle transport. *Macromol Biosci* 10(12):1473–1483.
15. Smart JD (2005) The basics and underlying mechanisms of mucoadhesion. *Adv Drug Deliv Rev* 57(11):1556–1568.
16. Kuhn SJ, Hallahan DE, Giorgio TD (2006) Characterization of superparamagnetic nanoparticle interactions with extracellular matrix in an in vitro system. *Ann Biomed Eng* 34(1):51–58.
17. Gillis RB, et al. (2012) Molecular weight distribution analysis by ultracentrifugation: Adaptation of a new approach for mucins. *Carbohydr Polym*, 10.1016/j.carbpol.2012.05.018.
18. Sarbolouki MN, Mahnam K, Rafiee-Pour HA (2004) Determination of pore/protein size via electrophoresis and slit sieve model. *Electrophoresis* 25(17):2907–2911.
19. Chrambach A, Rodbard D (1971) Polyacrylamide gel electrophoresis. *Science* 172 (3982):440–451.
20. Andrews GP, Laverty TP, Jones DS (2009) Mucoadhesive polymeric platforms for controlled drug delivery. *Eur J Pharm Biopharm* 71(3):505–518.
21. Florey HW (1962) The secretion and function of intestinal mucus. *Gastroenterology* 43:326–329.
22. Ruge CA, et al. (2012) The interplay of lung surfactant proteins and lipids assimilates the macrophage clearance of nanoparticles. *PLoS One* 7(7):e40775.
23. Lai SK, Wang YY, Hida K, Cone R, Hanes J (2010) Nanoparticles reveal that human cervicovaginal mucus is riddled with pores larger than viruses. *Proc Natl Acad Sci USA* 107(2):598–603.
24. Kirch J, Guenther M, Schneider M, Schaefer UF, Lehr C-M (2012) Computational fluid dynamics of nanoparticle disposition in the airways: Mucus interactions and mucociliary clearance. *Comput Vis Sci*, 10.1007/s00791-012-0184-x.
25. Gfeller KY, Nugaeva N, Hegner M (2005) Rapid biosensor for detection of antibiotic-selective growth of Escherichia coli. *Appl Environ Microbiol* 71(5):2626–2631.
26. Gastaldi AC, Jardim JR, King M (2000) The influence of temperature and length of time of storage of frog mucus samples. *Biorheology* 37(3):203–211.
27. Ziehl A, Bammert J, Holzer L, Wagner C, Zimmermann W (2009) Direct measurement of shear-induced cross-correlations of Brownian motion. *Phys Rev Lett* 103(23): 230602.
28. Cheezum MK, Walker WF, Guilford WH (2001) Quantitative comparison of algorithms for tracking single fluorescent particles. *Biophys J* 81(4):2378–2388.

Supporting Information

Kirch et al. 10.1073/pnas.1214066109

SI Text

Particle Characterization. Nanoparticles were characterized by nanoparticle tracking analysis. Measurements were performed with an LM10-HS (NanoSight). This technique was previously shown to be more precise in determining particle size distributions than standard dynamic light scattering, especially for polydisperse samples (1). Particle size distributions are displayed in Fig. S1.

Atomic Force Microscopy. Determination of adhesive interactions between mucin fibers and nanoparticles of different surface chemistry could be realized by force spectroscopy. Measurements of adhesion forces between nanoparticles and silica substrate allowed for an unbiased comparison between chitosan and PEG (2 kDa) -coated polystyrene (PS) nanoparticles. Particle adhesion to mucin fibers attached to the tip of the cantilever compared with their adhesion to the substrate, as shown in Fig. S2, shows that chitosan-coated particles adhere much stronger to the fibers than PEG-coated particles. Whereas the adhesion force between a mucin-functionalized tip and chitosan-coated particles was over 250% stronger than the adhesion force to the substrate, PEG coating of nanoparticles resulted in an even reduced adhesion compared with the bare silica substrate.

Capillary Penetration Experiments. Capillaries were fixed in a reproducible position next to the pole of the neodymium permanent magnet. A fit with the model by Chrambach and Rodbard was done according to equations described previously (2). Here, particle mobility in an external force field described as a function of gel concentration is given by (Eq. **S1**)

$$m = m_0 e^{-kc}, \qquad \textbf{[S1]}$$

where m is the particle mobility, m_0 is the mobility in water, c is the polymer concentration, and k is a system-specific constant.

Cryogenic Scanning EM. Along with the cryogenic scanning electron micrographs shown in the text (Fig. 3), additional images of horse mucus were taken in accordance with the method described (Fig. S3). These images verify the assumption of mucus being a heterogeneous material. In all pictures, very small pores of a few hundreds of nanometers can be seen, whereas in the same sample, comparably huge voids of multiple micrometers are present.

Optical Tweezers. The following additional information could be obtained from the mean squared displacements (MSDs) in mucus and hydroxyethylcellulose (HEC). In the HEC model, gel material homogeneity could be recovered not only from the uniformity of the MSDs at different locations within the gel (Fig. 4*B*) but also when considering displacements at a certain position in different direction (i.e., along the x and y axes of the pictures taken by the high-speed camera). As shown in Fig. S4*B*, both curves overlap almost completely. On the contrary, in mucus, strong deviations in the behavior of the MSD can be seen comparing the x and y directions of the trajectories (Fig. S4*A*). Comparing the values of the MSD along the y axis at 0.5 ms (Fig. S4*A*, dashed line) and 1 s (Fig. S4*A*, dashed/dotted line), there is only an increase by a factor of 3.25, whereas along the x axis, the values increase much steeper by a factor of 10. The variation in pore size becomes apparent when analyzing data from active oscillations as shown in Fig. S5. Although the strength of the optical trap was not changed compared with the measurement presented in Fig. 5 and the displacement of the trap was performed three times faster, the reaction of the bead to the trap was a lot stronger. Instead of tiny displacement amplitudes in the order of magnitude of less than 100 nm, here, the bead could be displaced about 750 nm in each direction.

The shear modulus was determined from the displacement data of beads that were confined in the focal region of the optical trap. This determination was achieved for mucus as well as the HEC model gel by a method proposed in 1997 in the work by Schnurr et al. (3), according to which the Fourier-transformed displacements are linked to the force spectrum of Brownian motion by a response function $\tilde{\alpha}$, the compliance. The compliance of non-Newtonian fluids is the complex function (Eq. **S2**)

$$\tilde{x} = \tilde{\alpha}^*(\omega)\tilde{F}_r, \qquad \textbf{[S2]}$$

where Fourier-transformed quantities are denoted by a tilde and the compliance is given by $\tilde{\alpha}^*(\omega) = \alpha'(\omega) + i\alpha''(\omega)$. Although the power spectral density $\langle|\tilde{x}(\omega)|^2\rangle$ of the particle displacements can be related directly to the imaginary part of the response function α'' by applying the fluctuation dissipation theorem (4) (Eq. **S3**)

$$\left\langle \left|\tilde{x}(\omega)\right|^2 \right\rangle = \frac{2k_BT}{\omega}\alpha''(\omega), \qquad \textbf{[S3]}$$

the determination of the real part α' is more extensive. By using the Kramers–Kronig relations (4), the knowledge of α'' allows for the calculation of α' by numerically solving the following principle value integral (Eq. **S4**):

$$\alpha'(\omega) = \frac{2}{\pi}P\int_0^\infty \frac{\omega\alpha''(\omega) - \zeta\alpha''(\zeta)}{\zeta^2 - \omega^2}d\zeta. \qquad \textbf{[S4]}$$

The denominator of the integral contains two singularities at $\zeta = \pm\omega$. Although the pole at $\zeta = -\omega$ plays no role for the integration, the pole at $\zeta = \omega$ must be avoided by excluding an infinitely small ε neighborhood surrounding ω from the integration, which is denoted by the letter P in the integration symbol. Finally, the connection between the compliance of the material with its shear modulus is given by (Eq. **S5**)

$$G^*(\omega) = \frac{1}{6\pi R}\cdot\frac{1}{\tilde{\alpha}^*(\omega)}, \qquad \textbf{[S5]}$$

where the shear modulus is given as $G^*(\omega) = G'(\omega) + iG''(\omega)$ with the elastic or storage modulus G' and the viscous or loss modulus G''. At this point, knowledge of the strength k of the optical trap is required, because it influences the elastic properties of the fluid over the whole frequency regimen in the form of an additive constant $G'_{\text{trap}} = k/6\pi R$ (5). In the case of the HEC model gel, these properties were determined directly out of the passive measurements using the equipartition of energy relating the thermal energy with the harmonic trapping potential (6). Because of the strong confinement by the polymer network, however, this method was not possible in mucus. Instead, the calibration of the trap strength was performed within a second sample cell containing water. The typical strength of the optical trap used in the experiment ranges was between 3 and 8 pN/μm. The frequency at which the corresponding apparent elastic modulus was reached also defined the lower data cutoff (typically around 1 Hz). The shear modulus at even lower frequencies would only represent the characteristics of the trap instead of the characteristics of mucus or HEC. As the upper cutoff, a frequency of 3.5 kHz was chosen, because it is well below the Ny-

quist frequency of, in our case, 8.192 kHz. This choice was motivated by the minimization of aliasing errors.

In conclusion, we find that the microrheology of mucus presents itself much more diversely than the microrheology of HEC. Although the mean spread of the storage modulus in mucus (Fig. S6*A*) covers a whole order of magnitude at each frequency over the whole frequency regimen, the fluctuations in HEC (Fig. S6*B*) are a lot narrower and typically do not move farther apart than a factor of two. The only exceptions are the moduli at lower frequencies than 20 Hz, which show a significant scatter. Similar information can be deduced from the loss moduli (Fig. S6 *C* and *D*), where the spread in the mucus data is even more significant. However, all results from microrheology imply a similar elastic as well as viscous behavior of mucus and HEC at all observed frequencies at least between 10 and 1,000 Hz. Additional agreement is found in the qualitative curve progression of both the storage and loss moduli. An interesting distinction between both materials is the fact that, in HEC, a cross-over of the elastic and viscous modulus can typically be observed near 100 Hz, whereas mucus does not show such a behavior.

1. Filipe V, Hawe A, Jiskoot W (2010) Critical evaluation of Nanoparticle Tracking Analysis (NTA) by NanoSight for the measurement of nanoparticles and protein aggregates. *Pharm Res* 27(5):796–810.
2. Sarbolouki MN, Mahnam K, Rafiee-Pour HA (2004) Determination of pore/protein size via electrophoresis and slit sieve model. *Electrophoresis* 25(17):2907–2911.
3. Schnurr B, Gittes F, MacKintosh FC, Schmidt CF (1997) Determining microscopic viscoelasticity in flexible and semiflexible polymer networks from thermal fluctuations. *Macromolecules* 30:7781–7792.
4. Landau LD, Lifshitz EM (1966) *Course of Theoretical Physics—Volume 5: Statistical Physics Part 1* (Pergamon, Oxford), 3rd Ed, pp 371–389.
5. Addas KM, Schmidt CF, Tang JX (2004) Microrheology of solutions of semiflexible biopolymer filaments using laser tweezers interferometry. *Phys Rev E Stat Nonlin Soft Matter Phys* 70(2 Pt 1):021503.
6. Simmons RM, Finer JT, Chu S, Spudich JA (1996) Quantitative measurements of force and displacement using an optical trap. *Biophys J* 70(4):1813–1822.

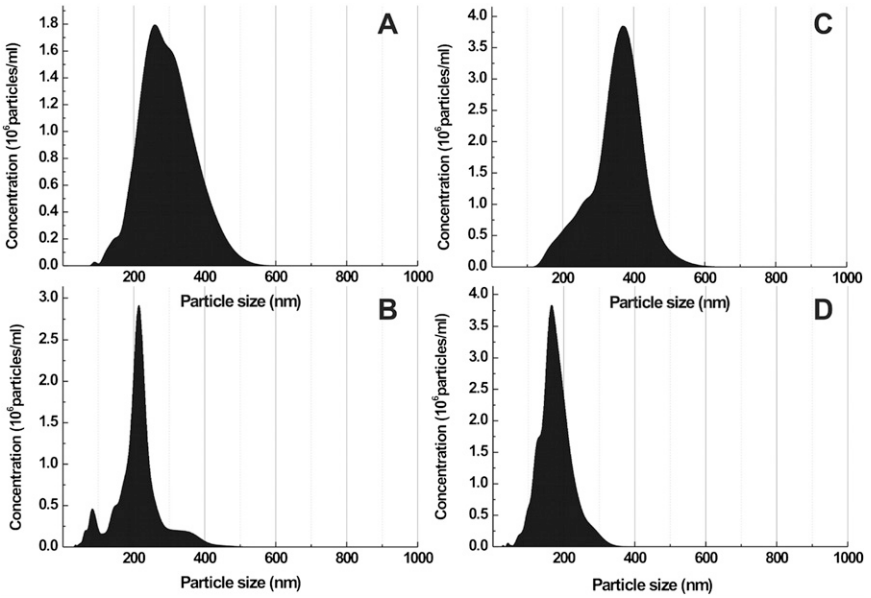

Fig. S1. Particle size distribution (hydrodynamic diameter) of polystyrene particles (*A* and *C*) and magnetic dextran particles (*B* and *D*) with 2 kDa PEG coating (*C* and *D*) or chitosan coating (*A* and *B*). Size distribution is averaged over $n = 3$ independent experiments.

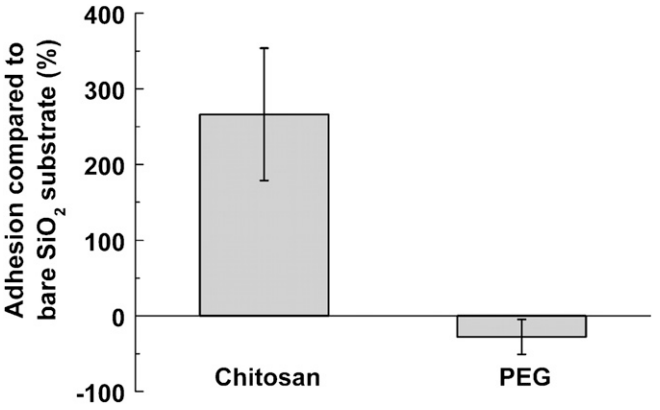

Fig. S2. Adhesion of differently coated nanoparticles to mucin fibers compared with underlying silica substrate. Data shown are mean ± SD.

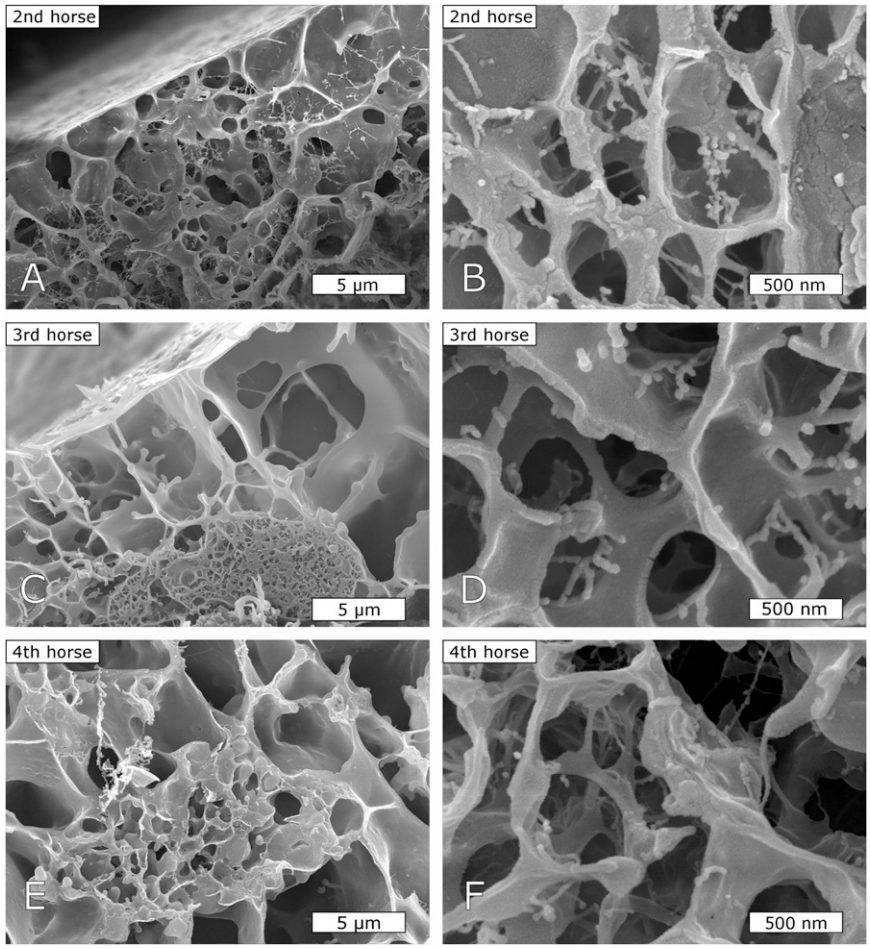

Fig. S3. Cryogenic scanning EM images of mucus from three additional horses in addition to the pictures in the text (Fig. 3 *D* and *E*). (*A* and *B*) 2nd horse. (*C* and *D*) 3rd horse. (*E* and *F*) 4th horse. (Scale bars: *A*, *C*, and *E*, 5 μm; *B*, *D*, and *F*, 500 nm.)

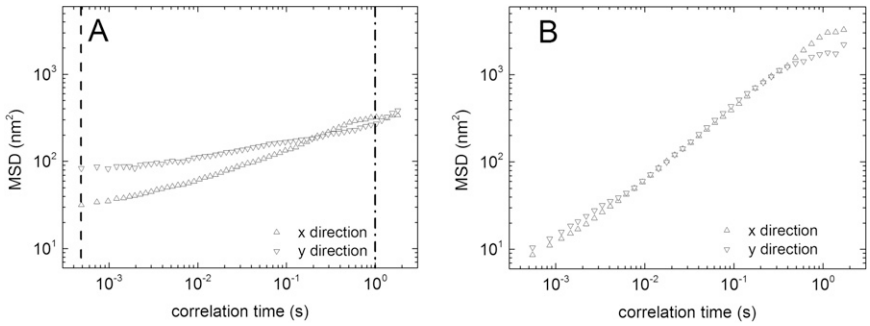

Fig. S4. The MSDs of the *x* and *y* directions are independently shown for beads in (*A*) mucus and (*B*) HEC. Although the isotropy and homogeneity of HEC can be deduced from the nearly identical curves that are recovered independent of the position within the fluid, the opposite is the case for mucus. The dashed and dashed/dotted lines in *A* denote 0.5 ms and 1 s, respectively.

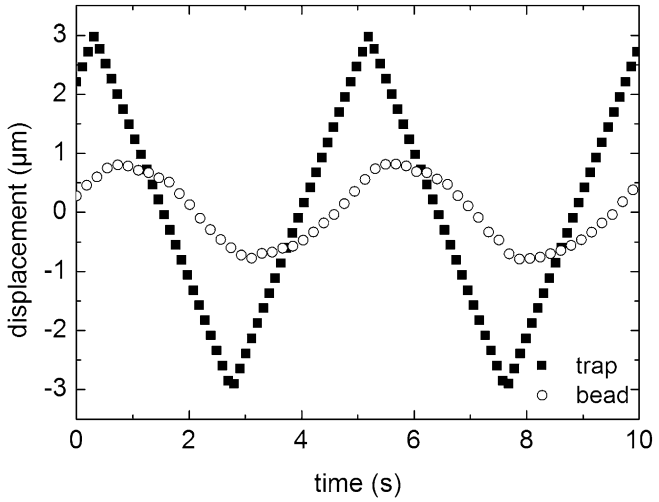

Fig. S5. The variety of reactions to an active measurement in the setup of optical tweezers within mucus is quite broad. Although a heavily constricted bead is shown in the text that is barely able to move, at a different position within the same sample, the beads could move more freely as shown here, referring to one of the larger voids within mucus. A displacement amplitude of the trap of 3 µm caused a considerable displacement of about 750 nm, whereas the trap strength was chosen in an identical way to the case presented in Fig. 5*A*.

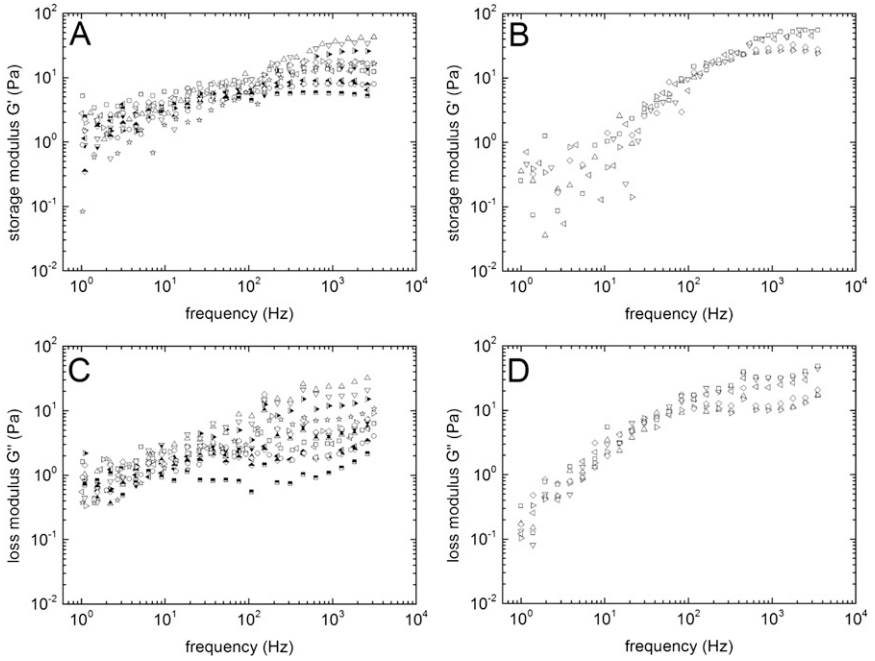

Fig. S6. Results from passive measurements at varying positions (denoted by different symbols) within (*A* and *C*) mucus and (*B* and *D*) HEC. The curve progression of the storage modulus G' (*A*) and the loss modulus G'' (*C*) of mucus is highly diverse compared with HEC (*B* and *D*), whereas the absolute values of G' and G'' range in a comparable order of magnitude. The strength of the optical trap was chosen between 3 and 8 pN/µm for all measurements.